Datum
2022-02-15

Dnr
2018-008054

Projektnr
47116-1

Energimyndighetens titel på projektet – svenska Optisk partikelmätning i avgasrör	
Energimyndighetens titel på projektet – engelska Optical particle measurement in exhaust system	
Universitet/högskola/företag Chalmers University of Technology	Avdelning/institution MC2
Adress Kemivägen 9, Se-412 96, Gothenburg	
Namn på projektledare Johan Liu	
Namn på ev övriga projektdeltagare Peter Enoksson, Per Lundgren, Agin Vyas, Mohammadamir Ghaderi, Jaco Visser, David Bilby, Lasse Simonson, Lisa Nyström, Ola Stenlåås, Nathan Kempema, Anna Lutz, Linus Kronlund, Thomas Lund	
Nyckelord: 5-7 st Particle measurement, optics, exhaust system, sensor	

Preface

The project has been funded by the Energy Council, together with Volvo Trucks AB, Volvo Cars AB, Scania AB, Ford Motor Company (USA) and Chalmers University of Technology AB. The main executing partner is the Electronics and Materials Systems Laboratory at Chalmers University of Technology, where system analysis, design and fabrication has taken place in close collaboration with the industrial partners, Ford Motor Company, Scania AB, Volvo Trucks AB and Volvo Cars AB. The system was evaluated for actual exhaust gas at various stages of the project at test stands at the industrial partners. The project duration is three years (2019-2021) and the total cost amounts to 6833 kSEK with 2000 kSEK contributed by industrial partners and 4833 kSEK requested from FFI.

Table of Contents

Contents

Preface 1
Table of Contents 1
Sammanfattning 3
Summary 3
Introduction and Background 4
Execution of the project 9
Project participants 12
Results 14
Round 1: 15
Design of optical window 15
Fabrication of optical window 17
Characterization 19

Box 310 • 631 04 Eskilstuna
Telefon 016-544 20 00 • Telefax 016-544 20 99
registrator@energimyndigheten.se
www.energimyndigheten.se
Org.nr 202100-5000

Packaging....20
Investigation of thermophoretic repulsion....20
Investigation of feasibility of regeneration....22
Discussion and conclusion....23
Round 2....25
Design....25
Fabrication of optical window....26
Packaging:....27
Characterization....29
Investigation of thermophoretic repulsion....29
Investigation of feasibility of regeneration....33
Discussion and conclusion....34
Publication list....35
References....35

Sammanfattning

Miljökonsekvenserna av utsläpp av nanopartiklar är ett allt större samhällsproblem. Som ett exempel har mätningar av partiklar (PM) varit lämpliga för att validera överensstämmelse med regulatoriska krav på bilars partikelutsläpp upp till Euro 4; i efterföljande versioner är emellertid också antalet ultrafina partiklar som släpps ut per km körning föremål för begränsningar, som inte kan valideras exakt med de konventionella PM2.5-metoderna, eftersom dess respons i hög grad domineras av de stora partiklarna i mätningen intervall upp till D_p = 2,5 µm.

Detta projekt handlar om genomförbarheten av att använda ett system för mätning av storleksfördelningen av nanopartiklar i avgaser (därav partikelnummer - PN) i området för partikeldiametrar på 40 nm <D_p <150 nm, med hjälp av optisk spridningsspektroskopi med flera detektorer. Mer specifikt mäts spektrumet av spritt ljus i våglängdsområdet mellan 250 nm och 800 nm vid flera vinkelpositioner i förhållande till en ljusstråle som infaller på avgaserna. Att underhålla ett optiskt genomskinligt fönster är en viktig aspekt och åtgärdas genom att undersöka sensorytans rengöring genom uppvärmning. Implementeringen syftar till att generera PN-data under användning för förbättrad motordriftskontroll och kontinuerlig validering av efterlevnad av utsläppsreglerna, vilka båda är väsentliga funktioner för användaren; fordonsindustrin.

I detta arbete beskrivs design, tillverkning och testning av prototyper av optiska fönster för att undersöka (sot) föroreningsreducering och självrengörande (regenerering) för applikationen i bilavgassensorer. Arbetet bedrevs i två omgångar; den första omgången ägnades åt designen och den första prototypframställningen av de optiska fönstren, medan den andra omgången implementerade olika optimeringar av designen och tillverkningen av nästa generations prototyp. 10x10 mm formar realiserades med optiska fönster bestående av inneboende poly-3C-SiC. Förpackning och trådlimning utfördes direkt på ett PCB och experimentella tester utfördes. Termoforetisk avstötning av sotpartiklar demonstrerades genom flera sotackumuleringsexperiment vid olika testplatser av bilindustrins partners. Det optiska fönsterpaketet skulle kunna installeras med stor överensstämmelse i installationen på olika fordonsplatser. Fönstren klarar höga spänningar på 85 V utan någon fysisk deformation vid 2W effekt. Den tål 43 V i 2041 minuter, 60 V i 66 minuter innan den går sönder. De termoforetiska repulsionsexperimenten visade att ett 43 V förspänt optiskt fönster var 40 % renare än det närliggande icke-förspända fönstret. Fönstren kan rengöras upp till 94 % vid 60 V i 20 minuter.

Summary

The environmental consequences of the emission of nanoparticles is an increasing societal concern. As one example, Particulate Matter (PM) measurements have been suitable for validating compliance with regulatory requirements on automotive particulate emission up to Euro 4; in subsequent versions, however, also the number of ultra-fine particulates emitted per km driving is subject to limitations, which cannot be accurately validated using the conventional PM2.5 approaches, because

its response is highly dominated by the large particles in the measurement range up to D_p= 2.5 μm.

This project is about the feasibility of employing a system for the measurement of size distribution of nanoparticulates in exhaust gas (thus Particle Number - PN) in the range of particle diameters of 40 nm< D_p< 150 nm, using multiple-detector optical scattering spectroscopy. More specifically, the spectrum of scattered light is measured in the wavelength range between 250 nm and 800 nm at several angular positions relative to a light beam incident on the exhaust gas. Maintaining an optically transparent window is an essential aspect and is addressed by investigating sensor surface cleaning by heating. The implementation is aiming for in-use generation of the PN data for improved engine operation control and continuous validation of emission regulation compliance, both of which are essential functions for the user; the automotive industry.

In this work, the design, fabrication and testing of prototype optical windows to investigate (soot) contamination mitigation and self-cleaning (regeneration) capabilities for the application in automotive exhaust sensors are described. The work was conducted in two rounds; the first round was dedicated to design and initial prototyping of the optical windows, while the second round implemented various optimizations to the design and fabrication of the next generation prototype. 10x10mm dies were realized with optical windows consisting of intrinsic poly-3C-SiC. Packaging and wire bonding were performed directly on a PCB and experimental tests were carried out. Thermophoretic repulsion of soot particles was demonstrated by multiple soot accumulation experiments at various test sites of automotive industry partners. The optical window package could be installed with considerable conformity in the setup at various automotive sites. The windows can sustain high voltages of 85 V without any physical deformation at 2 W power. It can withstand 43 V for 2041 mins, 60 V for 66 mins before breaking down. The thermophoretic repulsion experiments demonstrated that a 43 V biased optical window was 40 % cleaner than the nearby non-biased window. The windows can be cleaned up to 94 % at 60 V for 20 mins.

Introduction and Background

Emission of particles from the combustion engine in the automotive into the environment is in principle prevented using particulate filters [1]. PM sensors are typically placed after the filter and used to detect leaks in damaged filters which would exceed regulatory emission level thresholds. The three main groups of sensors for PM measurement are:

- Sensors based on light scattering, absorption or emission. Usually, the particle is used as a condensation centre in order to increase scattering cross section. These simple devices use a single light source and single angle of detection. The original size information is lost without pre-sensor size specification. This type of device is not currently implemented as an on-board diagnostic sensor;
- Sensors based on the measurement of the electrical current of deposited particles. Implementations often include high voltage in order to drive the amplification of deposited current into the femto-, pico- or nano ampere

range. Many of these devices rely on the mobility of electrically charged particles. This type of device is not currently implemented as an on-board diagnostic sensor;

- Sensors for measuring the electrical conductivity of particles that are deposited on a specially designed electrode structure. This type of device is commonly used on vehicle applications, however, does not provide information on particle size distribution.

State-of-the-art

Instrumentation based on light scattering from condensation-enlarged particles is used in a laboratory or dynamometer. In the absence of an aerosol size-classifier, such a condensation particle counter loses particle size information. Moreover, this approach has little potential for miniaturization due to the necessity for a reservoir of condensable liquid and constant flow. Therefore, it is not suitable for meeting the objectives.

Many common aerosol size measurement techniques are based on an electrical field [2]. For instance, an electrical mobility classifier, which is basically composed of two coaxially cylindrical electrodes, separates corona-charged particles. A DC high voltage ranging from 1 to 5 kV is applied to the inner electrode. The electric field formed between the electrodes makes the charged particles deflect radially outward at a rate determined by competition between electrostatic attraction and aerodynamic drag forces. Measurement of the electric current deposited by these mobility-resolved particles contains information on the size distribution of the particles. This strategy is the foundation of instruments like the Exhaust Engine Particle Sizer. However, the measurement results need to be carefully interpreted because of the dependence on the clustering of elementary particles. Such a cluster affects the charging and results in a complex aerodynamic behavior of compound soot particles. Moreover, controlled-flow rate gas sampling is required, and the measurement result requires measurement of femtoampere current levels. A typical measurement range includes particles between 6 and 450 nm. The combined effect of complexity (necessity for a pump) and limited potential for downsizing (long flow paths for size-speciation) limits its potential for meeting the objectives of the proposed project. Electrostatic soot sensors based on high voltage, after prioritizing simplicity over the ability for size speciation, have also been investigated [3]. These devices are not implemented in on-board diagnostic applications due to complications with maintenance of high voltage, electromagnetic signal noise, and isolation impedance necessary to measure pico-ampere currents in the corrosive, contaminant filled exhaust gas environment. Similarly, the common inclusion of a pump is impractical for long-term, on-vehicle use.

In the electrical conductivity sensor, the electrical conductivity between two interdigitated electrodes on the top side of a substrate is measured [1, 4-6]. A DC voltage is applied between the sensing electrodes, inducing an electrophoretic force, which attracts particles and results in particle accumulation on the sensor surface. The electrical current between the electrodes is proportional to the soot accumulation on the sensor surface, due to the high electrical conductivity of carbon. On the backside of the substrate is a heater structure, which is used to

periodically regenerate the sensor (i.e., clean the surface by burning away the accumulated soot) by heating up to several hundred °C.

Electrical conductivity measurement is simpler as compared to the mobility measurement. However, the sensor does not provide any information on particle size distribution. Moreover, the soot is deposited in the shape of very thin conductive 'wires', which are liable to break and thus result in non-reproducible measurement over time. Nevertheless, this type of sensor has demonstrated to be highly suitable for monitoring the health of diesel particulate filters in on-board vehicle diagnostic applications.

Optical techniques have also been investigated for measuring PM. Direct imaging of illuminated exhaust gas has been demonstrated to provide useful information on temperature distribution and particle sizing [7]. However, the result is only qualitative. Laser-induced incandescence (LII) is based on the use of a high-energy, pulsed laser to heat particles to very high temperatures, resulting in blackbody radiation that is proportional to the volume concentration of carbon in the particles [8, 9]. However, the use of a high-power laser makes the technique suitable for laboratory use only. Moreover, the measurement is complicated by issues such as the change in particle surface area during aerosol coagulation and the change in refractive index at soot deposition. Direct scattering of a laser beam is also used in a technique often referred to as laser diffractometry. Although the technique was originally intended for measurement of particles in µm to mm range, special techniques are generally implemented to extend the lower end of the measurement range down to sub-100 nm [10]. Direct scattering at the single laser wavelength at one small angle assumes Rayleigh scattering. Thus, the unintended operation in the Mie regime is effectively a source of error of this measurement technique. Since the approach proposed here actually uses the transition from Rayleigh to the Mie regime at increasing wavelength as essential information, this shortcoming of direct scattering can be considered one of the sources of inspiration that has led to the concept of measuring over a wide spectrum and at more than one angle, as proposed.

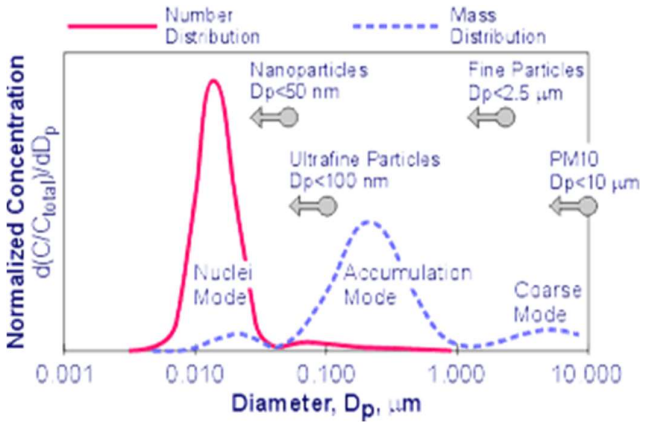

Figure 1: Typical particle size distributions weighted by number, surface area and mass, https://www.dieselnet.com/tech/dpmffsize.php

The typical size distribution of particles that are generated in a diesel engine is shown in Fig. 1. There are three peaks. The peak at several µm is not the result of the combustion process and is usually not considered. The peak at about 20 nm is due to the so-called 'dilution' of the emission gas with air at the exit of the exhaust, which results in condensation of elementary carbon particles and is relevant only in stationary operation of the engine. Only the peak at about 100 nm is due to the regular combustion process and is characteristic for emission at normal engine operation [11].

The number of small particles, which are proven to have a very adverse health effect [12], clearly hugely outnumbers the number of larger ones, but barely affects the measured total PM, because of the third-power relation between diameter and mass. Therefore, addressing the particle-initiated health concern requires the measurement of particle size distribution in real-time, which cannot be achieved by the traditional techniques described. Size-dependent particle scattering spectroscopy is explored in the proposed project as a new and powerful technique for achieving this objective. define and test optical scattering setups in work packages 1 and 2. An extensive effort and Ford and Chalmers was performed on simulating scattering, literature survey to understand and practice data inversion techniques, as well as designing, testing and iterating optical scattering setups for measurements with soot sizes and concentrations relevant for the project goal. However, this work will not be summarized in the report.

The proposed measurement principle is based on the different angular distributions of the scattering of light that is incident on a particle-containing gas, which is depending on the ratio between particle diameter and wavelength of the light. For a particle circumference smaller than the wavelength, the scattering is in the Rayleigh regime (primarily in the direction of the light beam, both forward and backward), while the scattering is in the Mie regime (more omni-directionally) for

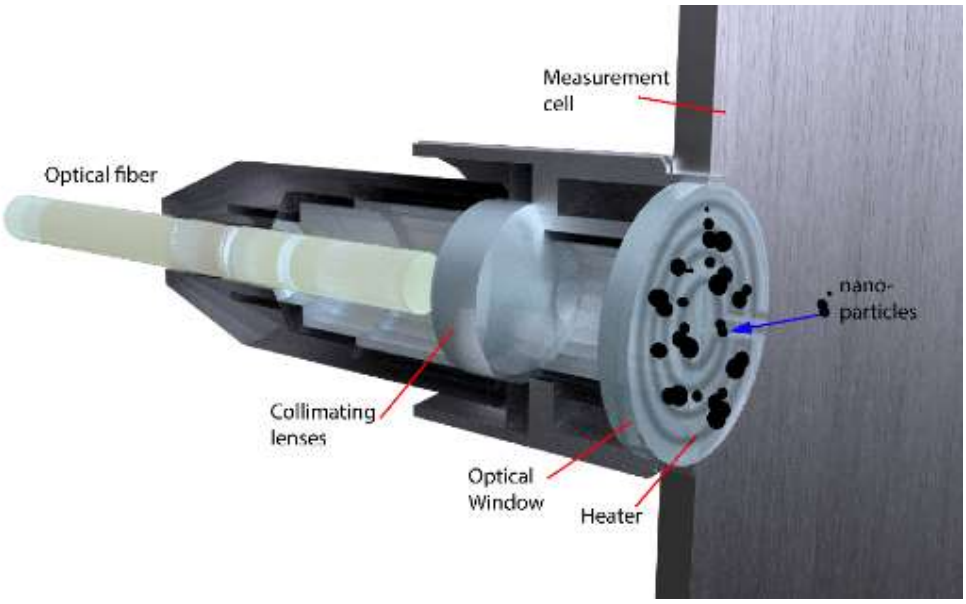

Figure 2: Artist's schematic illustration of the transparent interface to the exhaust pipe.

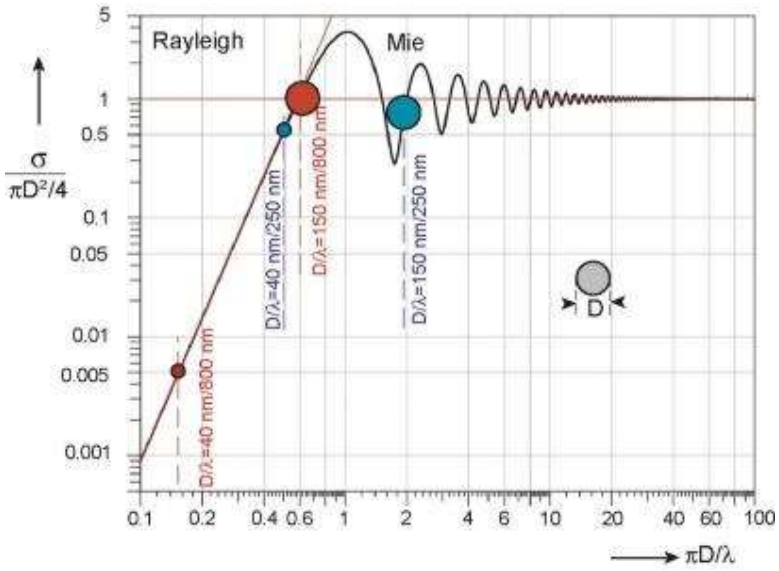

Figure 3: Principle of size-dependent particle scattering.

particles with a diameter much larger than the wavelength. In both modes the scattered light intensity increases with particle density, as known from radar technology on macroscopic objects. Nano-particle generation in a combustion engine peaks at about 80 nm. Particles with a diameter exceeding 50 nm are effectively captured in the particulate filter, but nano-particles remain, resulting in a peak in the actually emitted particles at about 40 nm. It is highly interesting (and relevant for meeting emission requirements) to detect particles down to 20 nm and beyond, but we addressed the range down to 40 nm within the frames of this project proposal. A key issue that has so far deterred automotive industry from using optical sensor systems in such a harsh an environment as the tailpipe is the contamination of sensing surfaces due to soot deposition. Addressing this issue is an important part of the project and we intend to systematically analyze the effectiveness of optical surface cleaning by periodical heating. The gained understanding in thus aspect is expected to be of fundamental general strategic importance when it comes it considering industrial implementation of optical sensing systems. Fig. 2 gives a schematic illustration of the issue and the primary way to address it i.e. adding a heating element.

For detection down to a particle size of about 40 nm we can apply the general theory of radar cross-section. Considering illumination of the particulate containing

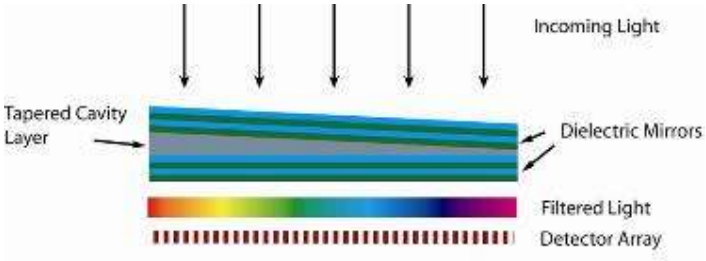

Figure 4: A Tapered Fabry-Perot LVOF for filtering the collimated light [14].

exhaust gas with 800 nm light, this results in maximum Rayleigh scattering for 150 nm diameter particles and less than 1% of that for 40 nm diameter particles, as is shown in Fig. 3. The effective absorption cross-sectional area is denoted as $\sigma/(\pi D^2/4)$. Therefore, the vertical axis basically indicates the effective area available for scattering relative to the physical cross-sectional area.

In the case of a 40 nm diameter nanoparticle, the absorption remains in the Rayleigh regime and the cross section increases with decreasing wavelength (D_p/λ increases) from 800 nm light to almost maximum Rayleigh scattering at 250 nm. For 150 nm diameter particles absorption is in the Mie regime. A spectral scan in the range from UV to near IR with detectors that are placed at several angular positions relative to the path of the incident light beam, provides the information on particle diameter distribution. The measurement principle is based on the different angular distributions of the scattering of light that is incident on a particle-containing gas, which is depending on the ratio between particle diameter and wavelength of the light. For a particle circumference smaller than the wavelength, the scattering is in the Rayleigh regime (primarily in the direction of the light beam, both forward and backward), while the scattering is in the Mie regime (more omni-directionally) for particles with a diameter much larger than the wavelength. In both modes the scattered light intensity increases with particle density.

We intend to use the Linearly Variable Optical Filter (LVOF) as the implementation of these microspectrometers [13]. The LVOF is basically a one-dimensional array of many Fabry-Perot (FP)-type of optical resonators as shown in Fig. 4. Rather than a huge number of discrete devices, the LVOF has a center layer (the resonator cavity) in the shape of a strip and a thickness that changes over its length as shown in Fig. 3. Bragg mirrors are placed on either side. Thus, the narrow passband wavelength of the LVOF varies linearly along its length. A detector array underneath the LVOF records the spectrum of the locally transmitted light. CMOS-compatible LVOF fabrication (e.g. processing temperatures < 400 °C) is based on reflow of a specially patterned layer of resist and a subsequent transfer etch of the tapered surface into a dielectric layer used as the resonator [14]. Implementation of this work is, however, out of the scope of the work.

Execution of the project

The project was carried out in a team of 4 persons for 2 years at the Electronics Materials and Systems Laboratory, MC2, Chalmers. A post-doctoral researcher was involved in the system design and realisation. Prof. Peter Enoksson (MEMS/MOEMS expert) supervised mainly this project till 2020. Prof. Johan Liu acted as the project leader since 2021 and Prof. Per Lundgren acted as co-supervisor and NEMS/CMOS expert. We also acknowledge the very kind support from Reinoud Wolffenbuttel.

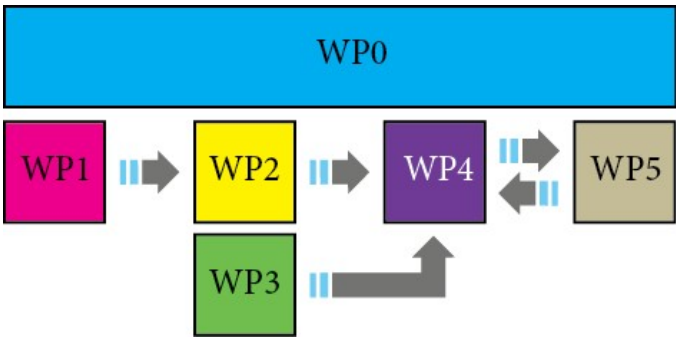

Figure 5: Organization of Work Packages.

The following work packages (WP's) were identified (Fig. 5)

WP0	**Project Management**
Leader (role and responsibility)	Chalmers (monitoring progress and reporting work done at Chalmers, keeping timeline, initiating meetings and resolving disputes)
Other participants (roles and responsibilities)	Ford (monitoring progress and reporting work done at Ford, attending consortium meetings) Scania (monitoring progress and reporting work done at Scania, attending consortium meetings) Volvo Cars (monitoring progress and reporting work done at Volvo Cars, attending consortium meetings) Volvo Trucks (monitoring progress and reporting work done at Volvo Trucks, attending cons. meetings).
Description of contents	Managing the other WP's, facilitating collaborations, ensuring in-time transfer of information and scheduling dissemination activities.
Method/approach (when relevant)	
Delivery	Active during the entire duration of the project

WP1	**Fundamental**
Leader (role and responsibility)	Chalmers (pursuing and managing the research, interacting with industrial partners)

Other participants (roles and responsibilities)	Industrial partners (interacting with research, giving feed-back on progress and priorities).
Description of contents	Study of the fundamental limitations of scattering spectroscopy in a gaseous medium and defining system specifications such as the detection limit at a range of particle diameters, minimum volume and number of spectrometers.
Method/approach (when relevant)	Literature study and simulations
Delivery	Mo 9

WP2	**Design**
Leader (role and responsibility)	Chalmers (pursuing and managing the research, interacting with industrial partners)
Other participants (roles and responsibilities)	Industrial partners (interacting with research).
Description of contents	Establish a basic design of a set-up based on discrete components and sub-systems.
Method/approach (when relevant)	Simulation; sub-system realisation and testing.
Delivery	Mo 12

WP3	**Integration**
Leader (role and responsibility)	Chalmers (managing the research, testing sample devices, interacting with industrial partners)
Other participants (roles and responsibilities)	Chalmers (investigating concepts for in-line soot removal by heating; preparing test sample devices). Other industrial partners (testing sample devices)
Description of contents	Investigating options for optical measurements in harsh environment by minimizing and removing contamination (soot and oil ash) on a surface that needs to be transparent. Establish a principal MEMS-based fabrication scheme including

	specifications of the materials and processes intended to be used.
Method/approach (when relevant)	Simulation, sample fabrication and testing.
Delivery	Mo 21

WP4	**Realisation**
Leader (role and responsibility)	Chalmers (managing the research and prototype fabrication, interacting with industrial partners)
Other participants (roles and responsibilities)	Other industrial partners (interacting with Chalmers; providing recommendations on practical restrictions)
Description of contents	Fabrication at the Chalmers MC2 facilities during months 6-12 and a second run during months 15-21.
Method/approach (when relevant)	Cleanroom fabrication.
Delivery	Mo 12 and Mo 21

WP5	**Validation**
Leader (role and responsibility)	Ford (managing the testing at the industrial partners and interacting with Chalmers)
Other participants (roles and responsibilities)	Other industrial partners (testing; interacting with Ford and Chalmers) Chalmers (providing input and assisting in testing)
Description of contents	Testing of prototype set-up at industrial partners. First version of the during months 15-18 and possibly a second version that is revised according to the findings of the first run during months 21-24.
Method/approach (when relevant)	Testing at test set-up.
Delivery	Mo 18 and Mo 24

Project participants

The Department of Microtechnology and Nanoscience at Chalmers, Gothenburg. MC2 of Chalmers has an extremely well-equipped infrastructure for

micro- and nanofabrication. The 1200 m^2 clean room contains state-of-the-art equipment for dry etching, material deposition (metal and insulating thin films can be deposited by a number of evaporation and sputter systems) and furnaces for thermal processes (low-pressure chemical vapour deposition, oxidation, drive-in and anneal after implantation etc.) applied to silicon wafers up to 150 mm in diameter. Equipment for preliminary wafer-level testing is available. Moreover, equipment for extensive optical testing, such as a general-purpose optical test bench and spectrometer with high resolving power and covering the entire spectral range of interest are available.

Ford Research and Innovation Center (Ford RIC) in Dearborn, MI, USA. Equipment for producing stable ultrafine particle size distributions was available, such as a Jing miniCAST 5201c propane-burning soot generator as well as a TSI 3076 atomizer (which can prepare non-soot aerosol). Moreover, reference instruments for characterizing aerosols, such as a Pegasor particle sensor, DustTrak, a scanning mobility particle sizer (SMPS), an electrostatic particle impactor (ELPI), a microsoot sensor (MSS, based on a photo-acoustic principle) and an aerodynamic particle sizer (APS), was available for validation of early demonstrators of the particulate sensor based on scattering spectroscopy. Ford R&A in Dearborn has a state-of-the-art Vehicle Emissions Research Laboratory (VERL) with extensive exhaust gas and PM instrumentation and 2 vehicle roll dynamometers. Moreover, 10 engine dynamometers may be available to piggy-back prototype sensors at the final phase for testing at real-world conditions.

Volvo Trucks AB acted as an industrial partner providing input regarding the investigated technology for industrial applications. We also supported in the validation of the technology by providing test cell possibility. Here we used Volvo's internal particulate number measurement instruments to be used in parallel with the technology developed in the project for validating the technology in an experimental test cell setup.

Volvo Cars was able to support with equipment measuring particle number and size in real time (Cambustion DMS-500 and TSI EEPS) as well as on-board particle number instruments for Real Driving Emissions (AVL Move). In addition to vehicles, Volvo Cars also has engines that were used for prototype testing of the sensor.

Scania CV AB contributed with:

A) Reference group of three engineers with high experience in PM/PN/PD-measurement in test bench and on vehicle.

Reference group activities and deliverables:

Review sensor design, review test plans, be discussion partner for the academic partners to ensure industrial relevance and to report the endurance test.

B) An endurance test of four weeks intended to give a first indication on the sensors ability to handle post exhaust treatment engine exhaust gases and exhaust conditions. The test was conducted in an engine test bed.

Available resource and performed activities:

Endurance engine test bed four week test (one out of two parallel tests in the test bed) of 1-4 prototypes, including test preparation, test decommissioning and reference measurement of sensors under relevant conditions before and after the test.

Deliverable: Indication on sensor concepts capability to function in the post exhaust treatment environment of a heavy-duty engine included in D5.

Results

The objectives of this work were as follows:

1. Design an optical window (schematic in Figure 6) fabricated in a CMOS compatible cleanroom and which is able to be heated electrically up to soot oxidizing temperatures.
2. Ability for the entire package to withstand ambient temperatures of 450 °C, analog to the case in a car exhaust.
3. The optical window should be as large as possible but should at least have a diameter of a few microns.
4. Investigate the thermophoretic repulsion during in-situ soot deposition experiments.
5. Feasibility of regeneration of the optical transparent SiC windows.

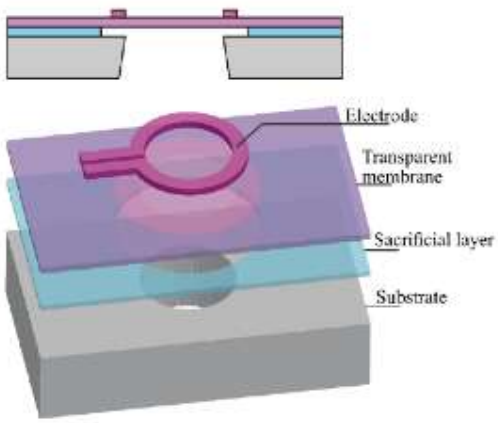

Figure 6: Schematic design of the optically transparent "self-cleaning" SiC windows fabricated on a solid-state substrate

The results of the project are described based on the objectives of the project of designing a robust optical window that can be electrically heated to soot oxidizing temperatures, fabrication of these chips in a CMOS compatible cleanroom, devising a packaging that can withstand 450 °C temperatures, the in-situ testing of the packages for thermophoretic repulsion and regeneration of transparent SiC windows.

The project results are divided into 2 rounds of experimental work and characterization. The first round was conducted from 2019 – 2021, with characterization experiments conducted at Ford. The design of the optical window was simulated in COMSOL Multiphysics for stress, varying voltage ranges, and particulate matter distribution through thermophoretic effect. The optical window was fabricated and tested at Ford and Volvo cars. The results of the window were analyzed for thermophoresis and regeneration and conclusion were drawn for improving the stability of the design.

The second round was conducted from 2021 – 2022, where characterization experiments were conducted at Chalmers, Volvo Trucks and Scania. The design of the optical window was optimized based on the first round's considerations. A wafer scale fabrication process was developed with a high yield. The device was packaged in an aluminum housing with an ability to withstand high temperature up to 450 °C without any defects. The package was tested on-site at Volvo Trucks and Scania.

Round 1:

Design of optical window

The structure is basically composed of a suspended optically transparent membrane. An electrically conductive layer on top is patterned into a resistor and can be used for heating of the membrane. The heater is optically transparent for effective use of the entire membrane area as a window. In case of significant differences in optical transmission between the membrane- and the heater material, or differences in their wavelength dependencies over the spectral range considered, a design that blocks the light at the position of the latter is to be used to avoid a wavelength-dependent average transmission throughout the window area. Bulk micromachining of the silicon substrate in a deep reactive ion-etching (DRIE) process is applied for fabrication of the dielectric membrane that is to function as the optical window.

A small to moderate tensile stress is desired in order to achieve a taut (i.e., flat, non-buckled) membrane. The dimensions of the membrane result as a compromise between the minimum aperture required for passing a practical light beam, and the maximum diameter that can be sustained when considering residual stress in the

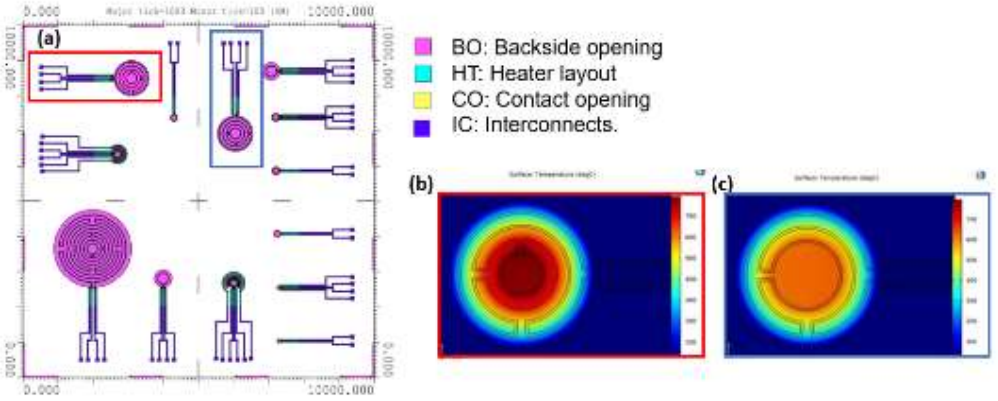

Figure 7: (a) Designed chip for optical window, (b) Lateral temperature distribution on a MEMS window for 4 heater loops and (c) 3 loops at 3 W.

layers that comprise the membrane and its thickness. The absolute value of the tensile stress increases with increasing dopant concentration in the poly-SiC layers considered.

The SiO_2 layer functions as the landing layer for the through-wafer etch, and its thickness was chosen to be 2 µm. In order to yield a membrane with minimal optical extinction, its thickness is kept to a minimum. A uniform temperature profile is desirable for optimal operation of the transparent window, with minimum membrane area occupied by the heaters. Moreover, power efficiency is considered. Limiting heat diffusion from the membrane to the surrounding rim implies that the outer part of the heater should be at a certain distance from the rim, which makes a compromise between a uniform temperature profile and low power dissipation inevitable. Three-dimensional finite element analysis (FEA) using measured material properties and considering realistic flow conditions was applied to analyze the geometry of the heater and membrane. The layout design was optimized for uniform temperature at a given power dissipation using COMSOL Multiphysics. Various simulated chip designs are shown in the chip pallettee shown in Figure 7(a). The heat loss due to conduction in the membrane and the gas and convection through the fast-flowing gas above the membrane were considered, while the radiation loss was estimated to be much smaller than the conductive loss and was ignored. Moreover, the temperature coefficient of resistivity (TCR) of the undoped SiC is not considered in these simulations. These assumptions limit the validity of the simulations to the lower operating temperature range. The membrane diameter was kept constant at 1000 µm and the temperature profile of a heater with a different number of turns is shown. The width of the wires was 20 µm.

LPCVD is used for deposition of an intrinsic SiC film and a highly doped SiC film. The sheet resistance of the deposited films was measured using the four-point Kelvin measurement. Based on the high difference between the resistivities of the intrinsic SiC (about 440 Ω·cm) and the highly doped SiC layer ($\rho = 3.36 \times 10^{-3}$ Ω·cm), it can be calculated that the current densities in these layers differ by three orders of magnitude. Based on the large separation of the electrical bulk resistivity between the intrinsic and the highly doped version of the poly-SiC layer, it was decided that a passivation layer in between the heater and membrane layers is not necessary, thus favoring fabrication convenience. These values were included in the finite element model (FEM) for analyzing the different heater designs at realistic conditions and the results are shown in Figure 7 (b-c). At 3 W constant injected power, the structure with more heater loops generates a higher peak temperature at its center. Most implementations are based on four-loop heater designs, for enabling a peak temperature in excess of 700 °C for more than 40% of the membrane area in case of a diameter exceeding 1000 µm.

Fabrication of optical window

Once the designs were finalized, the fabrication process was design to manufacture the optical windows on 10 mm x 10 mm chips. The flowchart is based on the design described in this section and a schematic representation in included in Fig. 8 and 9.

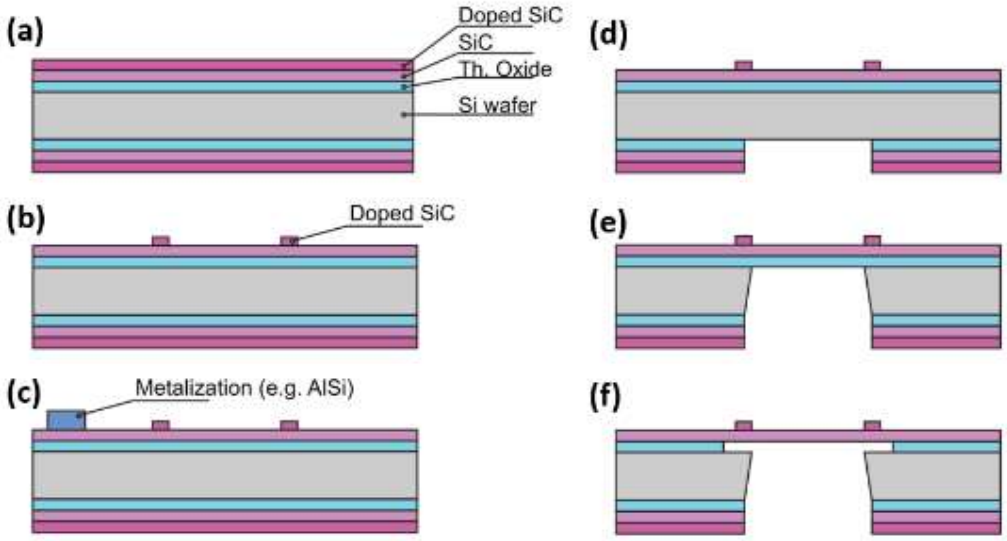

Figure 8: Schematic fabrication process of the optical sensor: (a), Growth of Thermal Oxide, LPCVD deposition SiC window, and N-doped SiC device layer. (b), Heater pattern definition: Lithography/ Dry etching (c), Metallization and IC definition: AlSi, W, Ti (d), Backside window opening: Lithography/ Dry etching (e), Through wafer etching: DRIE (f) Vapor HF etching

As starting material a silicon wafer is chosen. It would be most pragmatic to use double side polished (DSP) wafers, because back-side processing is required. SSP wafers are diffuse on the backside and complicates lithography. Standard zero-layer processing is performed, after which on the wafers 2 µm thermal oxide is grown. This layer results in thermal isolation between the substrate and the subsequent carbide layers.

After the thermal oxide, two poly-SiC depositions are followed. The undoped carbide layer is used as optical window later, while the doped layer is patterned to form the heater structure. It was found that over the entire batch of 25 wafers, the thickness of the undoped carbide membrane layer varies from 500 nm to 300 nm (Figure 8(a)). After the three thermal depositions, the FRONTSIDE of the wafer is coated with 4:0 µm AZ3017 photoresist without Edge Bed Removal (EBR). The standard resist is used because only a relatively thin layer poly-SiC needs to be etched, namely 500 nm. Another advantage is that the coater/developer station EVG120 can be used by doing so, which yields a more reproducible process compared to manual coating. Lithography is performed using 700 mJ/cm^2 to be able to etch the heater structure out of the doped poly-SiC layer (Figure 8(b), 9(a)). After the heater structures have been formed, the wafers were stripped and standard Si cleaning was performed. A HF dip was performed to get rid of any native oxide in

0.55% HF and the wafers were rinsed and dried. The wafers were deposited with 500nm AlSi(1%). Both depositions were carried out at 350 °C to yield the best metallization quality and to increase the chance for some interface reaction between the poly-SiC and the metal (Figure 3(c), 9(b)). After the metalization, the backside of the wafers was coated with 4:0 µm AZ3027 photoresist and IM1 BS openings was exposed.

The hard mask on the backside consisting of the thermal oxide and the two poly-SiC layers was opened in phases. First, the poly-SiC was etched with the Omega ICP etcher, using the Chlorine/HBr recipe at 25 °C recipe. The etching tool was used with a Cl/HBr recipe, because the etching uniformity was less of a concern in this step, this etching would land on the thermal oxide anyway. The thermal oxide

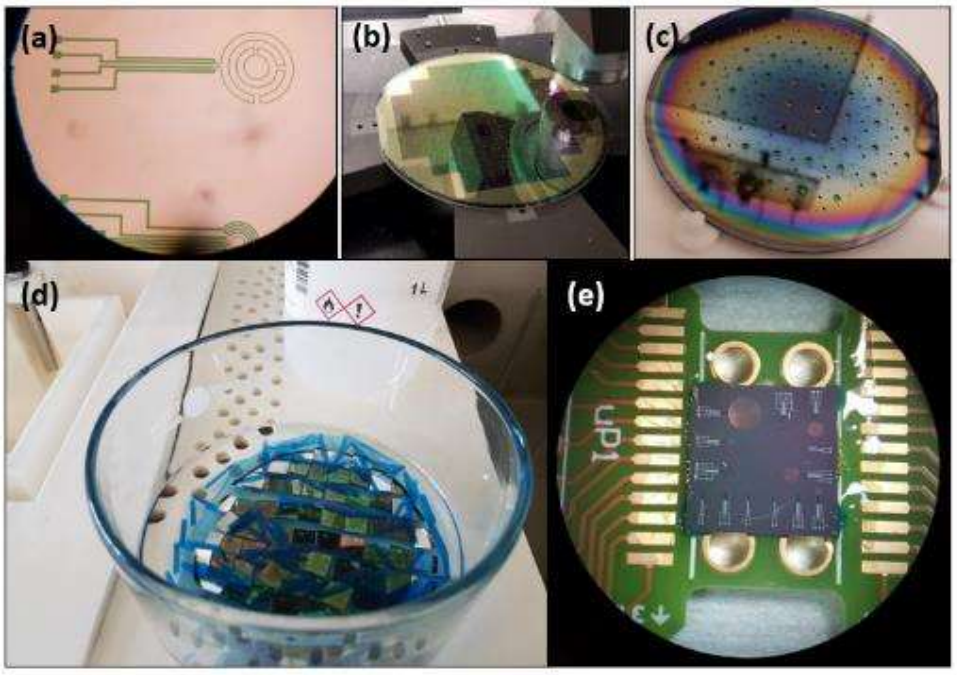

Figure 9 (a) Heater definition, (b) metallization, (c) through Si wafer etch, (d) dicing, (e) wire bonding.

was subsequently opened using wet- chemical etching with 1:7 BHF (Figure 8(d)). To protect the metalized frontside of the wafer at this point, the front side of the wafers was coated with 1:4 µm without EBR and developed with a recipe using only baking steps. Etching through the wafers was done with the Rapier using recipe 0EKL smooth 20 °C. The number of cycles used was determined iteratively. P1 was etched for 739 cycles, P2 for 900, and P7 for 840 cycles. The 900 and 840 cycle etching resulted in etched bare silicon, caused by the BACKSIDE hard mask being not thick enough (Figure 8(e), 9(c)). After the through wafer etching, first an oxygen plasma was needed to remove the residual PR and the passivation material in the cavities. It is important to remove the thermal oxide used as landing layer as soon as possible after through wafer etching. Due to the stress mismatch, the membranes are brittle while handling. For the wafers with aluminum IC, the vapor HF tool could easily be used. 4 cycles of recipe 3 of 300 s each was used and

appeared successful (Figure 8(f)). The aluminum wafers were spray coated after this release step to enable dicing foil removal from the thin membranes by using an acetone rinse, later on during the dicing and packaging steps shown in Figure 9(d - e).

Characterization

The goal of these devices is to heat the membranes, functioning as optical windows, up to well-defined, predictable and measurable temperatures. In order to achieve this, the injected amount of power should be linked to a certain temperature. Because it is expected that the DC resistance of the heaters is a function of temperature, an over calibration measurement is carried out. In this measurement, the PCB with soldered wires is put in an oven. The temperature in the oven is ramped up in steps of 10 °C while simultaneously the DC resistance is measured. The temperature at the location of the silicon die is measured with a thermocouple. Both the thermocouple and Keithley SMU read-out was done using LabView. The voltage used for reading out the resistance was 200 mV to prevent self-heating. A schematic of the used equipment is included in Fig. 10(a). Based on the initial heating tests, it was found that membranes named M9 and M10 were most promising based on the mechanical robustness and thermal homogeneity over the membrane. Therefore, M9 and M10 were calibrated in this test. The stepwise increase of the temperature was done to have well-defined coarse steps in the ramping temperature. This would help linking the measured impedance data to the temperature data, in case the relation between both would have been weak. The maximum temperature to which was ramped equals 195 °C. The results of the resistance vs temperature characterization is shown in Fig. 10(b).

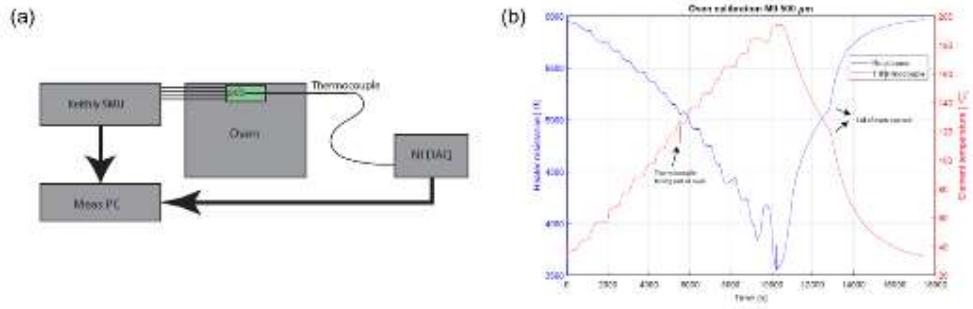

Figure 10: (a) Schematic figure of the measurement setup. (b) Resistance vs temperature measurements conducted in the oven.

The stepwise increasing temperature is clearly visible, along with the consistently decreasing resistance. As can be noted are the temperature and resistance measured both during ramping up the oven temperature as during cooling off. The spike in the measured temperature around 5500 seconds is the result of the thermocouple falling out of the oven. The discontinuity of the slope in the measured resistance during the cooling off phase is caused by the lid of the oven being opened. When the temperature is plotted against the measured resistance to investigate the effect between both quantities. Clearly distinguishable is the stepwise increase in the temperature and the smoother decrease in temperature. Additionally, lay both ramps not exactly on top of each other. Both effects indicate that still a temperature

difference existing between the thermocouple and the silicon substrate. In general, it can be said that a decreasing resistance is yielded when temperature is increased.

The same inference can also be concluded from literature that the resistance goes down with increasing temperature, yielding a negative TCR. This corresponds to the findings in this work. The absolute value of the TCR is a function of the doping concentration and thus the resistivity. The lower the resistivity, the smaller the TCR in absolute value, but with a larger linearity. The drop in resistance over a temperature range from 20 °C to 200 °C is around 50-60 %, which corresponds to the findings in this work. The TCR measured in this work is in the same order of magnitude as reported in literature [2] [3]. The reported TCR by Noh et al. is with 0.002 close to the measured values in this work.

Packaging

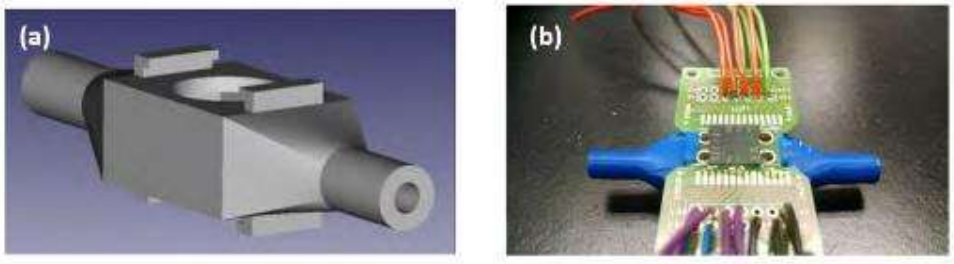

Figure 11: (a) 3D printed housing for the optical sensor. (b) Final device package with sensor on wirebonded PCB

The flow housing was designed by D. Bilby, Ford and subsequently 3D-printed. It was designed in such a way that the PCB could be clamped to the opening, while enabling a lateral ow of soot rich gas through the housing. The housing has openings on the front and bottom side, against which the PCB under test and a Perspex window was installed respectively. Having the additional opening on the bottom side of the housing enables future optical transmission measurements while the sample is exposed to soot. An improvised sealing between the housing, the PCB and the Perspex was facilitated by using clay. The housing and the final device package is included in Fig. 11.

Investigation of thermophoretic repulsion

For the soot accumulation measurements, the entire die was exposed to the soot rich ow while the transparency was monitored with an optical camera, including a USB camera. In Figure 12, a schematic overview of the setup is included. A Jing Minicast is used to generate the soot, where the different setting can be used to vary the size distribution of the generated soot particles. The dilutor is used to be able to control the soot concentration, where two the ejector and dilutor flow do control the final dilution ratio. From the dilutor, two lines go to the reference measurement tools, the DustTrak and the Microsoot Sensor. A third line goes to the sensor sample under test, which is inspected through an optical microscope. One of the membranes is heated using a Keithley SMU in 4 point measurement configuration, the flow is controlled downstream of the sensor using an MFC.

The flow rate used for the preliminary measurement is equal to 1 L/min, translating to a lateral flow of 200 mm/s After preliminary experiments it was found that even after exposure of more than 4 hours, not an clearly distinguishable amount of soot was visible on the backside of the heated and non-heated membranes. The M12 membrane was biased with a fixed current, yielding a temperature of 70 °C. After the exposure, which was carried out over night, microscope images were taken using back light from both the heated as the non-heated M10 membranes. It can be

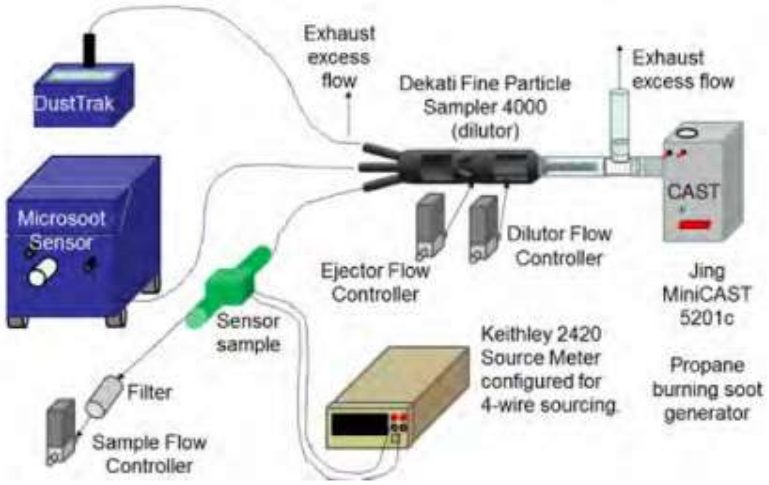

Figure 12: Device validation setup

concluded from this result that even the relatively small temperature difference of the membrane with respect to the temperature of the exposed gas, results in a convincing difference in the amount of deposited soot. It can further be noticed that most soot is deposited in the center of the non-heated membrane, while there is a ring-shaped area where the window stay clear.

The effect of thermophoretic repulsion can clearly be distinguished between M10 and M12 in the Figure 13, where M10 is the heated membrane while M12 is not. The soot is deposited in a realistic scenario on M12. When M10 is inspected from the backside, along the edge of the cavity, a large amount of soot was deposited. At the same time, no soot particles were observed on the surface of the membrane.

Investigation of feasibility of regeneration

After being able to keep an optical window clean from soot particles, the second objective to achieve is to regenerate the membranes. More specifically this means removal of the present soot by oxidation caused by elevated temperatures. It is

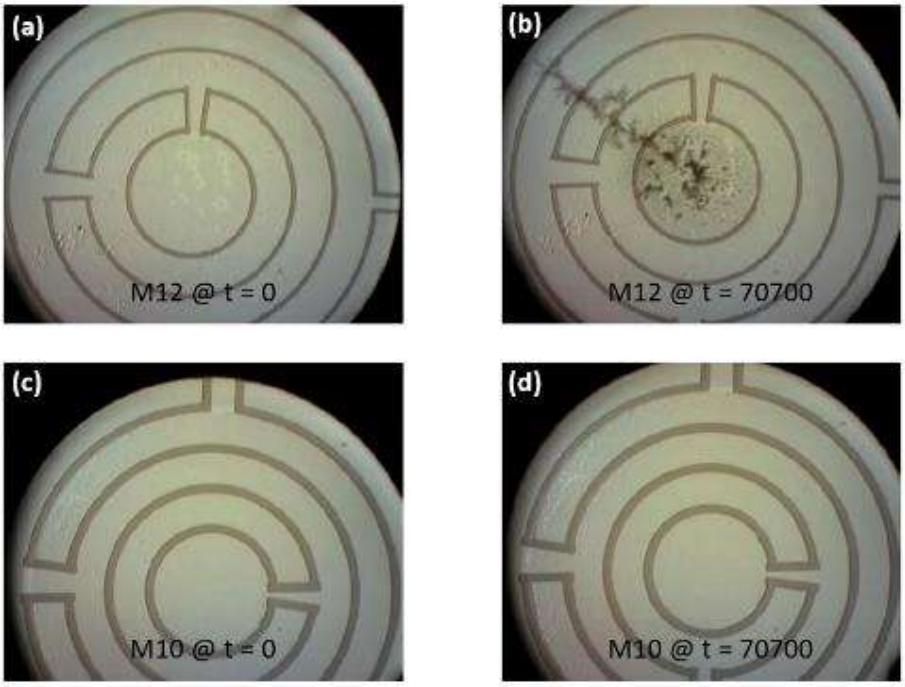

Figure 13: Regenerable windows heated M10 and unheated M12 over the course of soot flow.

known from experience that the soot regeneration reaction is an abrupt function of temperature. 500 °C is the temperatures where the soot regeneration process starts.

After the first measurements, another run was carried out. This time the flow rate and soot concentration were set such, that immediate deposition takes place. In this thermophoresis measurement, membrane M10 was heated while M12 was not heated. Both of these membranes have a diameter of 1000 µm, such that M12 can be used as reference for the M10 membrane. Before the soot deposition, the membrane/heater structure of M10 was calibrated using the FLIR optical camera in

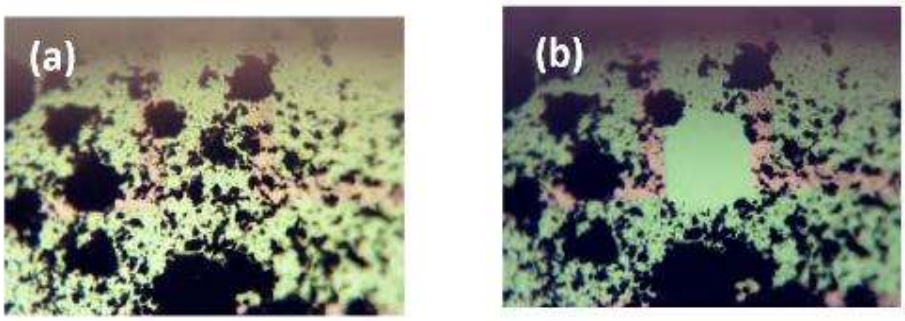

Figure 14: (a) M9 before and (b) after regeneration test.

combination with the Keithly SMU. The soot total deposition time was 70 700 s which equals 19 hours and 38 minutes. During this time, pictures were taken at fixed intervals, which enable data processing later.

The first membrane on which the regeneration attempted, is M9 with a diameter of 500 μm. Soot dendrites have been grown on and in the region around the hotspot. This soot is deposited by diffusion, showing a dendrite structure. This represents a realistic deposition scenario and the dynamic effects during deposition, caused by the flow and resulting turbulence, are included in the soot deposition pattern. Because of the finite resistivity at elevated temperatures of the membrane layer, regeneration should be performed by exploiting the available hotspot. The current was ramped up, even up to temperatures where the membrane start glowing at the hotspot. This glowing results in a local permanent change of the material, which appears to be a buckled region. The regeneration is illustrated by Fig. 14.

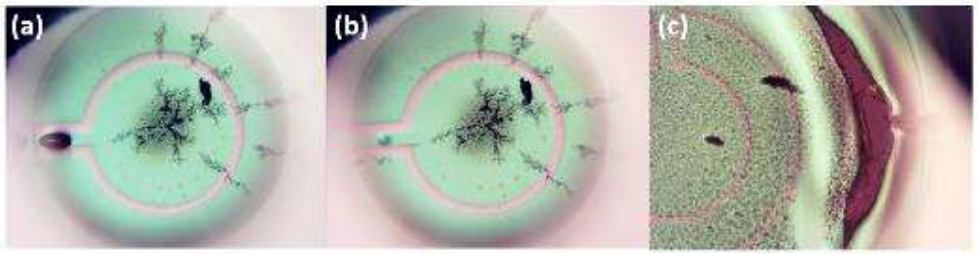

Figure 15:(a) Permanent deformation in M9, (b) Buckling in M9, (c) Rip in M12 after heating till glow.

When the injected power passes a certain threshold value, which is depending on the membrane under test, the membrane starts glowing. Although in the previous section it was demonstrated that regeneration can be performed within a reasonable time, in this case below 3 minutes, without entering the operating range where the membrane starts glowing, for research purposes it is still interesting what happens if the power is pushed way beyond this range. In some regeneration experiments, where the soot was not on or close to the hotspot, this pushing was even desired to increase the temperature in the region around the hotspot. The buckling of the membrane is visible, caused by the highly local heating of the membrane. After cooling down the M9 membrane back to room temperature, permanent deformation is visible. More intense glowing was observed when M12 was pushed to the limit, after which is ripped. The results of buckling and rips are shown in Figure 15. Disturbed stress distribution (tensile to compressive with buckling) in combination with changed material parameters causes this ripping action to happen.

Discussion and conclusion

The MEMS optical membranes in SiC fabricated in this work provide preliminary validation of their suitability as transparent MEMS platform with a view into the soot-containing exhaust gas. Restoring window transparency by heating at about 600 °C (mode 1 operation) has been essentially demonstrated. Although the regeneration operation was limited to small hot spots, the results show effective removal of soot from the window, thus restoring its transparency. Moreover, thermophoresis for maintaining a transparent window has been demonstrated for

heating to 35 °C above the soot-containing gas temperature. It should be emphasized that these results are preliminary, as the experimentation was carried out using a CAST soot generator for generating a particle flow close to room temperature. High temperature survivability was shown by the regeneration tests, where no permanent material change was observed, nor shifts in the device performance from an electrical or mechanical point of view.

The MEMS heater design was adequate for repeatedly demonstrating the effect of thermophoretic repulsion of soot particles in the exhaust gas. Surface regeneration was demonstrated by oxidation of severe contamination by impacted soot. Regeneration was achieved for a hot spot area of about 1000 μm^2 in less than 5 min, without any permanent damage or deformation to the membrane. Power dissipation for a hotspot of about 40 µm is 30 mW, which is equivalent to 6 $\mu W/\mu m^2$, as compared to 0.95 $\mu W/\mu m^2$ used in the simulations. The difference is mainly due to the small spot diameter and an improved agreement in case of full-membrane heating is expected. Visual inspection showed that transparency was maintained after the regeneration. The occurrence of hotspots during deposition implies that a dielectric isolation layer between the membrane and heater poly-SiC layers is required for a larger and more homogeneously heated membrane.

Round 2

The work in round 2 revolves around optimization of optical window design and fabrication process, followed by aluminum packaging for high temperature endurance and device testing at various automotive partner test rigs.

Design

In the Round 2, in 2020-21, we designed a second version of MEMS-fabricated devices of the regenerable window design which gives full-control and high uniformity of the membrane temperature profile required for effectively keeping the window transparent.

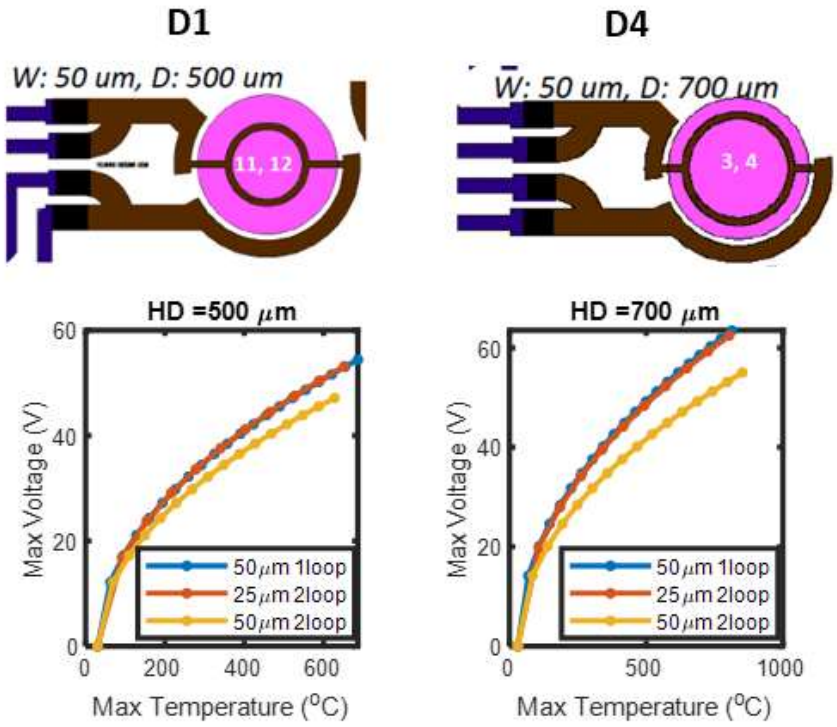

Figure 16: Simulation of round 2 optical windows for robust membrane heating

This is a simple membrane structure with one heater loop over the membrane. The heater is powered using two interconnects at either side of the membrane. In this analysis the heater width is set to 50 μm while its diameter is varied from 500 to 700 μm. The temperature and buckling of the membrane are analyzed. Although we have assumed many simplifications in the model, the calculation of the buckling as a function of applied power (hence temperature) quickly becomes computationally challenging. To solve the convergence, load ramping method was used. In this method, the parameter that causes nonlinearity (here applied power or voltage) is ramped from small values and each solution is used as a starting point for the next parameter. As long as a small enough step is considered the problem converges. The modeling of the heated membranes showed that the deformation of the membrane and the stress does not significantly improve the resilience of the

membrane. The results for optical windows named D1 and D4 are shown in Figure 16.

In none of the various heater configurations that was studied no optimization was observed. The (max) stress build up in the membrane increases rather linearly with the average temperature over the membrane. The fabrication masks designs were then updated for window size of 500 μm and 700 μm. The layer thicknesses were changed with the new heater routing design to improve the robustness. An additional SiN insulating layer was added between the SiC window and doped SiC heater trace to avoid the buckling and rupture failures that the earlier devices experienced.

Fabrication of optical window

The fabrication process of the optical windows follows the previously described fabrication process in Round 1 with the addition of SiN growth step in the initial thin film stack, and increased thickness of SiC for improved robustness. The packaging for deep reactive ion etching (DRIE) is also improved. In the first version of fabrication, we suffered from poor thermal contact in DRIE process leading to burn-off of photoresist. Device yield suffers due to poor masking, however, we managed to etch the backside. Poor thermal contacting leads to etching of SiO_2 at the top-side causing membrane breakage. Etched marks for dicing are cleaved however chips break at unwanted locations and the pressure from diamond scribing causes membranes to break. Therefore, there was a need to address the challenges in thermal taping. We had envisaged a wafer-bonding process through photoresist.

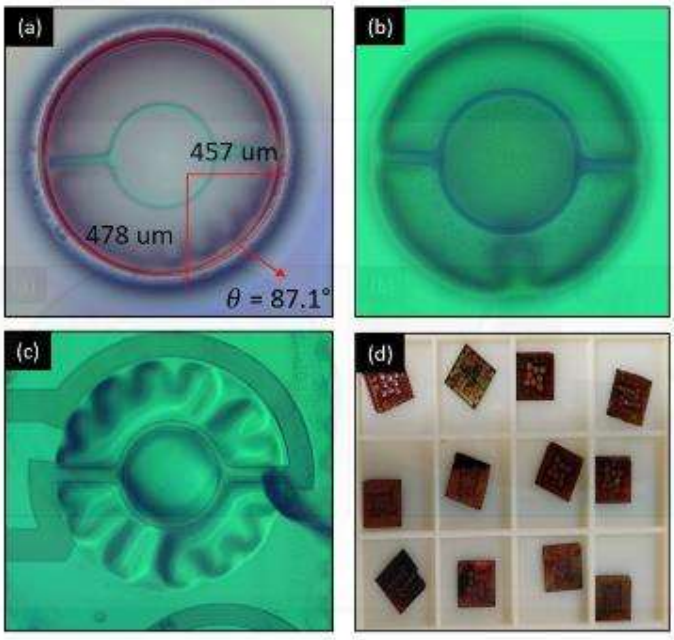

Figure 17: (a) Heater structure from backside after DRIE etching, (b) Heater structure after SiO2 etch, (c) Top side of heater-window, (d) fabricated chips after dicing.

For the next version, we used the new packaging technique by using a thick photoresist the package the 4” wafer on a 6” wafer. A photoresist package was used to attach the 4” Si wafer to a 6” Si/SiO_2 wafer. Fig. 17(a) shows the results from fabrication after DRIE process and SiO_2 etch. The tapering angle for DRIE etching was measured to be 87°. Once satisfied with the DRIE process, dicing was performed on the wafer package using height sense. Dicing vertically after horizontal processing is tricky. The photoresist underneath is heated and it melts causing chips to fly away in the tool. The processing was paused and the strips were manually broken in to chips as seen in Fig. 17(d).

Packaging:

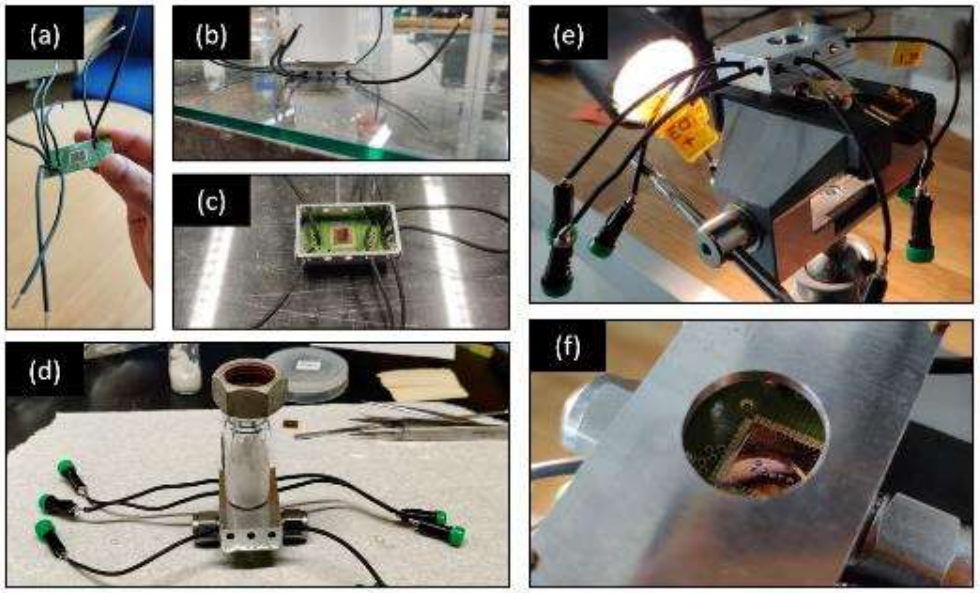

Figure 18: (a) Soldered wires to the chip-PCB packages, (b) Gluing the aluminum body to the package using Resbond 906 glue, (c) Soldering 4 mm female banana connecters to the soldered wires (d) Gluing the package to Swagelok cell (8 mm diameter) (e) Optical inspection of soot pathway, (f) Image with an optical focus on the chips in the MWP.

The chosen chip is glued to the high temperature PCB using Resbond 906 glue. The glue is prepared by mixing Resbond 906 power and binder in a 100:44 ratio. The glue is poured over the PCB and chip bounded to it while applying 50 N from top. The glue is dried for 2 hours at room temperature and then cured at 350 °C for 2 hours. High temperature silicon wires are soldered to the wire bonded PCB chip package for measuring four devices in-situ as shown in Fig. 18(a). A custom made aluminum package is glued to the PCB surface with soldered wires coming out of holes (Fig. 18(b)). The second terminals of soldered wires are attached to 4 mm female banana connecters for plug-and-play during in-situ conditions. The aluminum PCB package is glued to the Swagelok cell using the same gluing

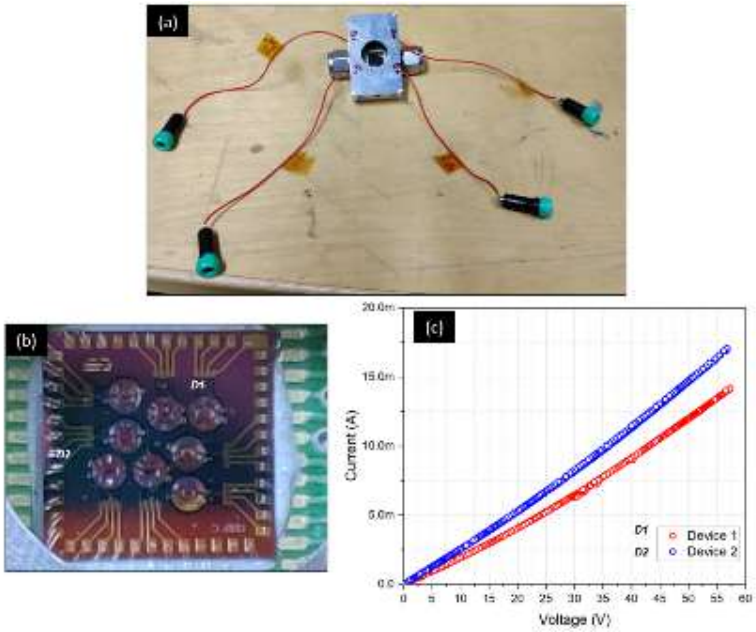

Figure 20: (a) MWP delivered to Scania, (b) Chip embedded in the package, (c) Characterization of the optical sensors on the chip package.

technique as used for the chip PCB bounding with added weight on top as seen in Figure 18(d). In Figure 18(e, f), we analyze the path of soot by looking at light pathways through the windows. We will call the combination of fabricated chip with windows wire bonded to the high temperature PCB, encased in an aluminium body on a Swagelok cell as the Micro window package (MWP1).

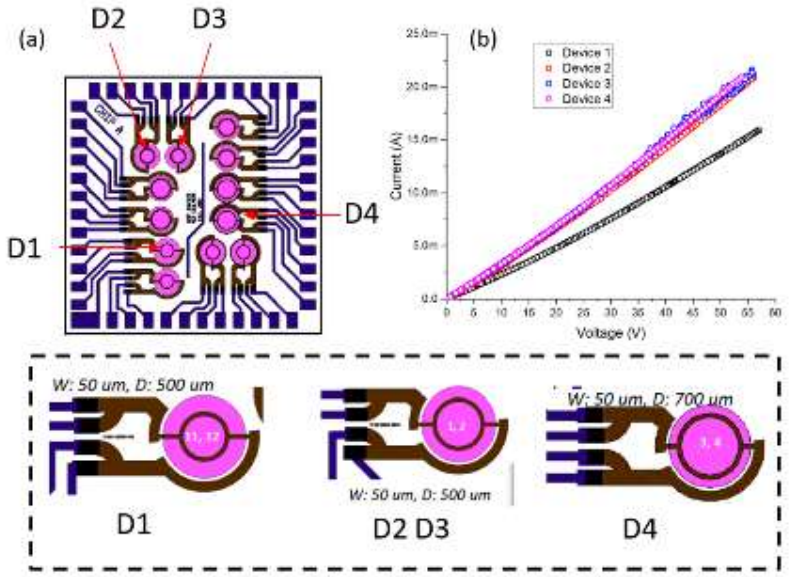

Figure 19:(a) Schematic design of the chip used in Micro Window Package (MWP) delivered to Volvo Trucks, (Device description in dashed box) (b) Current response of the heater under various applied potentials.

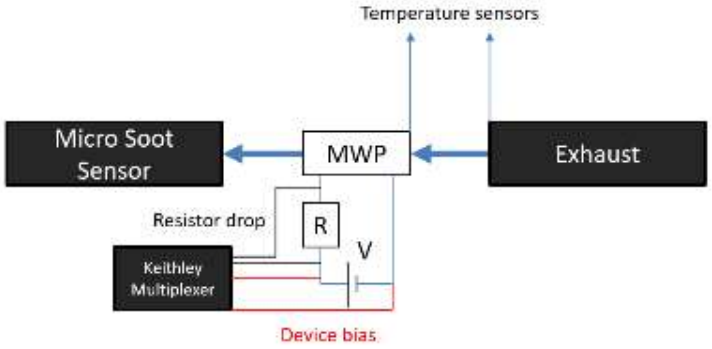

Figure 21: Configuration of measurement setup at Volvo Trucks

Characterization

The MWP1 package was characterized after packaging. The chip bounded used in the package is shown in Figure 19. The current response of the four devices D1, D2, D3, and D4 are shown in Figure 19(b).

Another set of the packaged device shown in Figure 20(a) is delivered to Scania named MWP2. The manufacturing process of the package is similar to the one constructed for Volvo trucks. The chip containing optical sensors is shown in Figure 20(b) with the two devices used for testing labelled as D1 and D2. The devices are characterized before delivery. The result for current measurements are shown in Figure 20(c).

Investigation of thermophoretic repulsion

The MWP1 package is tested at Volvo trucks at one of their latest engines. The MWP1 is connected to the AVL micro soot senor through a 6 mm stainless steel pipe. The other end of the MWP is connected to a flexible Teflon pipe with a temperature sensor lead inserted inside. Figure 21 shows the image of the setup. The temperature at the exhaust was measured at 176 °C, and the temperature inside the Teflon pipe is measured at 46 °C. The cylinder temperature is measured to be ~

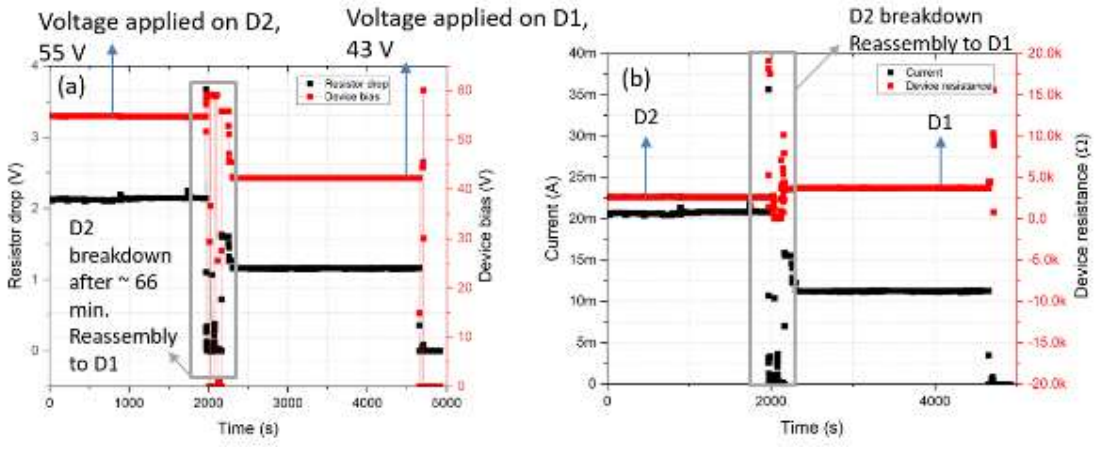

Figure 22: Voltage settings for the test duration at Volvo Trucks (a) Resistor drop measured on R (left) and Device bias (right), (b) Current in the heater (left) and measured device resistance (right)

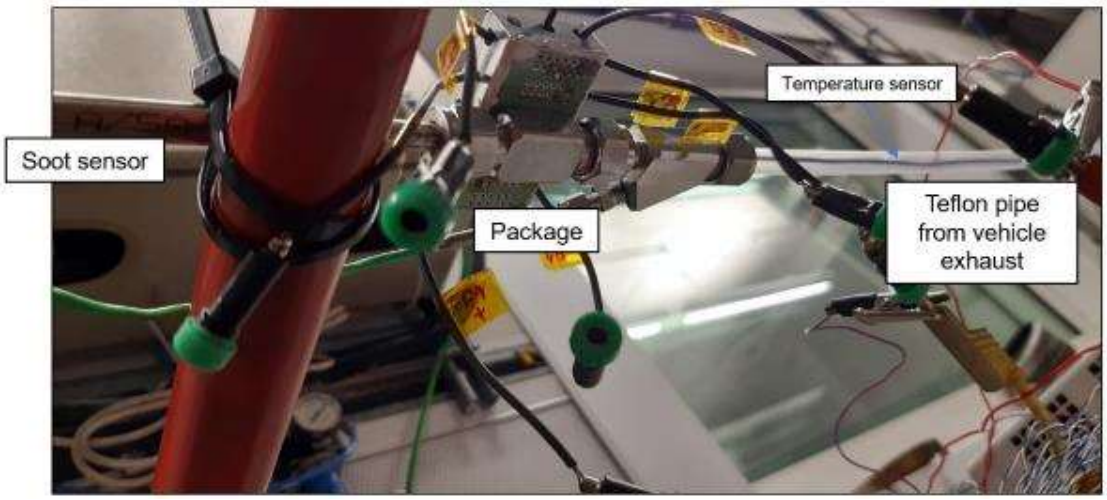

Figure 23: Test setup at Volvo trucks

200 °C. The flow rate in the MWP1 is measured as 7500 ml/min. The amount of soot detected in the AVL soot sensor is shown in Figure 24. The red trends in the graph represents the concentrations present in the current run while the trends in blue demonstrate a normal exhaust behavior of the engine. Thus, we can conclude that the MWP was subjected to a high concentration soot flow.

The MWP1 has four devices with external leads as shown in the schematic Figure 21. Devices D2 and D3 are identical and best suited for comparative assessment. Thus, D2 was connected to the power supply at 55 V to observe the thermophoretic effect at high temperatures. D2, however breaks down after 66 mins at 55 V. The observed destruction of D2 includes breaking of SiC windows. Furthermore, the fluttering windows during soot flow create a short circuit in D3 which is the closed device to D2. Thus, breakdown of D2 led to malfunction of D3 as well. The setup was later changed to D1 as shown in figure 23. The setup of a single device at Volvo Trucks is shown in Figure 23.

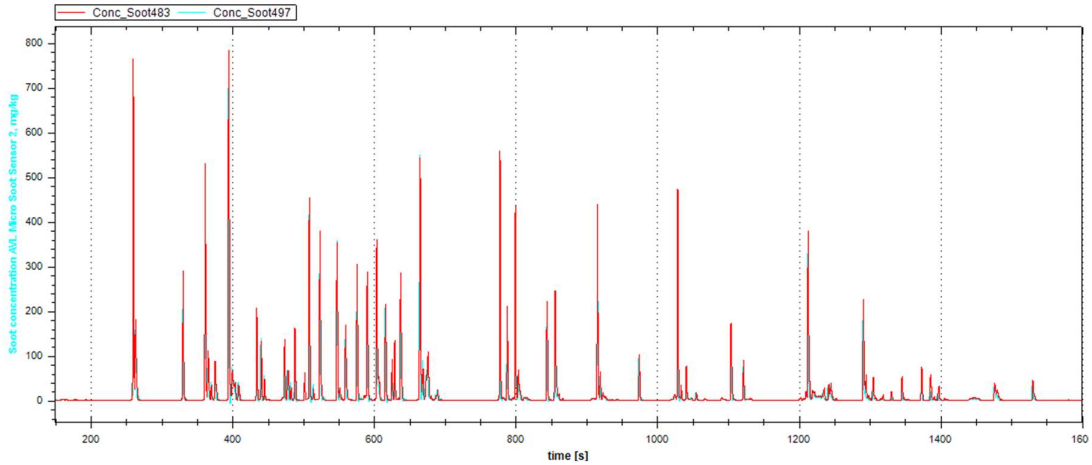

Figure 24: Analysis of soot as captured in the Micro soot sensor after two rounds of soot flow. The red and blue lines show a similar trend demonstrating uniformity in soot flow.

D1 was then connected to the power supply. However, this time the voltage was kept to 43 V, barely enough to see a glow at optical inspection. Figure 22 shows the voltage, current and resistance of D2 and D1 at different voltages. On completion of the soot generation cycle, the MWP was unmounted from the exhaust setup and it was retrieved back to Chalmers for further investigation.

The second objective of FFI project involved investigation of thermophoretic effect on the soot flow across the windows through the Swagelok. The observed thermophoretic effect on the MWP in-situ is shown in Figure 25. The package after soot cycling is shown in Figure 25(a). We can see black streaks across the PCB. This leakage present in the packaging leads to breakdown of connection between the PCB and Swagelok. Also, since the temperature of the soot inside Swagelok was measured to be about 45 °C, we can assume formation of water droplets. Presence of water in the adhesive reduces its bonding strength by several orders of magnitude. On inspection of the package through zoomed lenses, we can see a slight

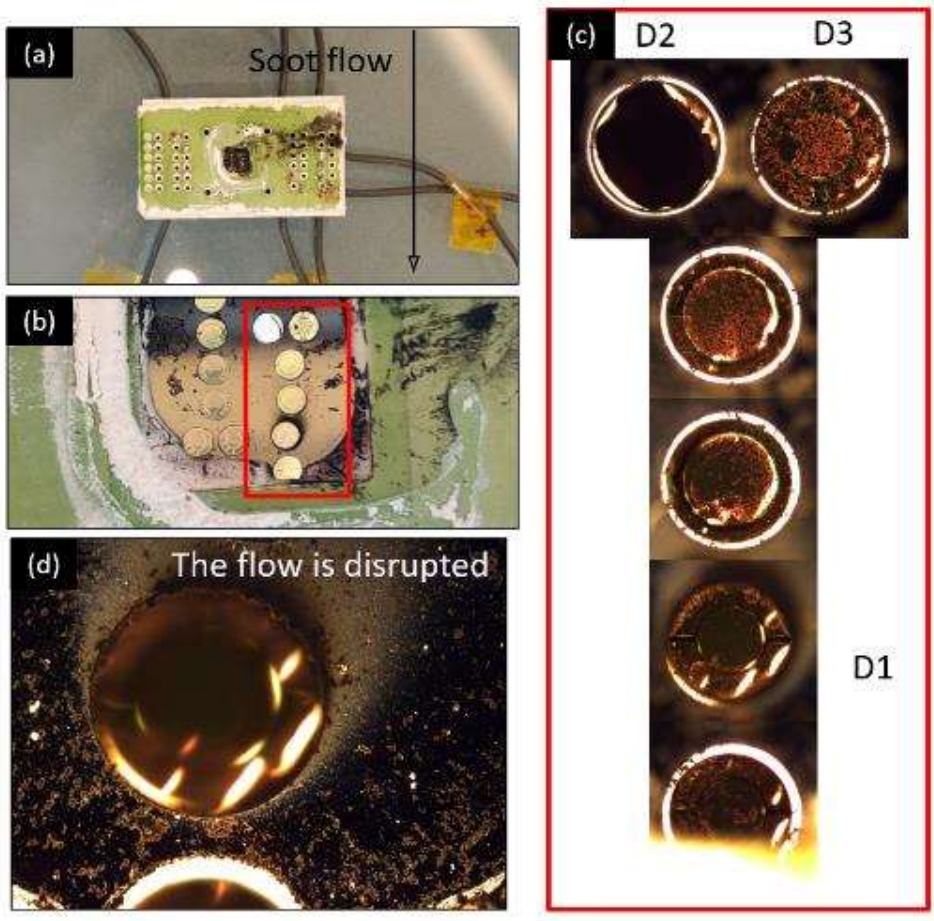

Figure 25: (a) MWP after soot cycling, (b) Zoomed image of the chips directly in-line of the soot exhaust, (c) Optical microscope images of the windows just after testing in-situ, (d) Optical micrograph of the backside surface of the chip after soot cycle demonstrating the thermophoretic effect on soot flow.

distinction in the optical transmission pattern. The red section in Figure 25(b), can be seen in Figure 25(c), observed under an optical microscope. As we can clearly

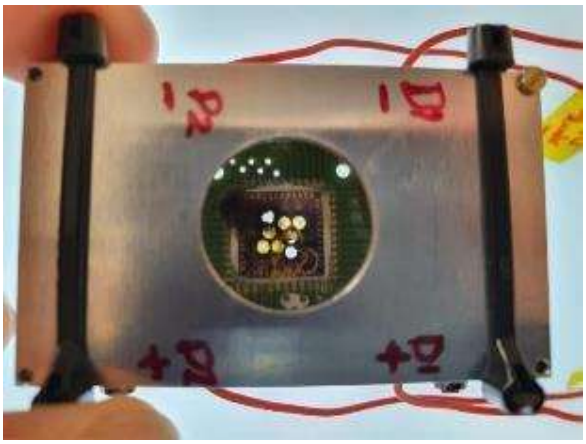

Figure 26: Destroyed windows at testing at 40 V.

see, there is a pattern in terms of soot deposition validating the thermophoretic effect in the optical windows. As D1 is connected to a potential difference of 45 V, it is the cleanest window among the column of devices. Going one device upward or downward, we see that there is more soot deposited at the edges further away from D1. Similarly moving two devices upwards from D1, we observe a high soot deposition. Similarly, for broken D3. That device has soot deposited and agglomerated on the surface.

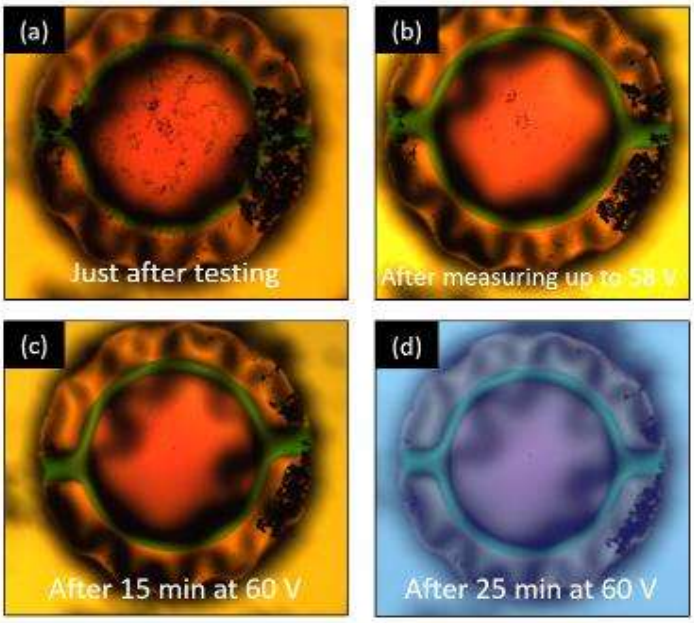

Figure 27: D1 heater (a) after testing, (b) after first round of test, (c) After 15 mins at 60 V, (d) after 25 min at 60 V

For the MWP2 tested at Scania, the sensor had been powered-on and off 38 and 39 occasions and had a total operation time of 16h 24 min and 17h 37 min (both at 40 V). Visual inspection (see Figure 26) reveals that both the powered sensor windows were destroyed during the test campaign. Reviewing the operator log the first sensor

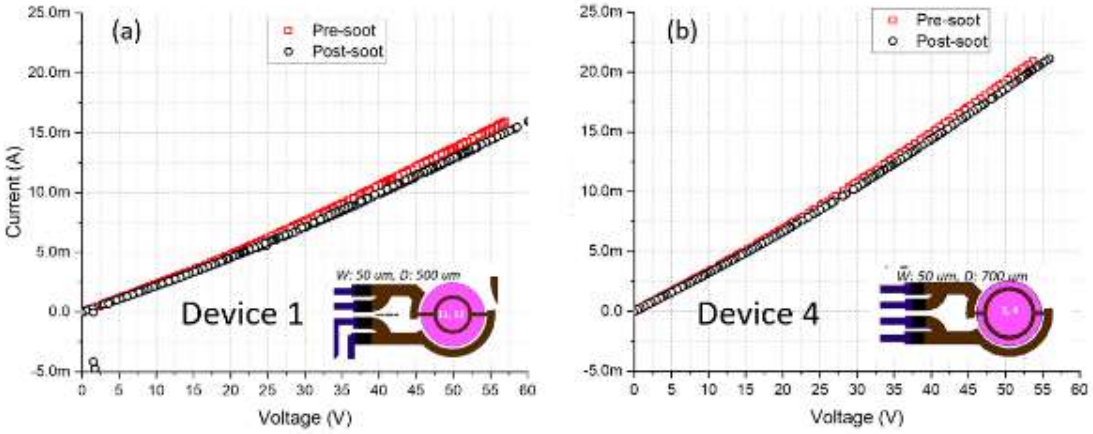

Figure 28: Pre- and post-soot characterization of (a) D1 and (b) D4.

window malfunctioned either when powered off or before/at power on and the second sensor window before or at the next attempted start up.

The package 2 was replaced with MWP1 (the one used at Volvo) and, the windows D1 and D4 were powered at 43V.

Investigation of feasibility of regeneration

To address the issue of cleaning the contaminant deposition, the devices D1 and D4 on the MWP are probed with Keithley power supply, first to measure the change in resistance of the devices, and secondly to burn of the contaminants. Figure 27 shows the device responses from 0 – 58 V. The decrease in resistance can be attributed to dendrite formation on the SiC films. These streaks of soot are visible in Figure 27(b).

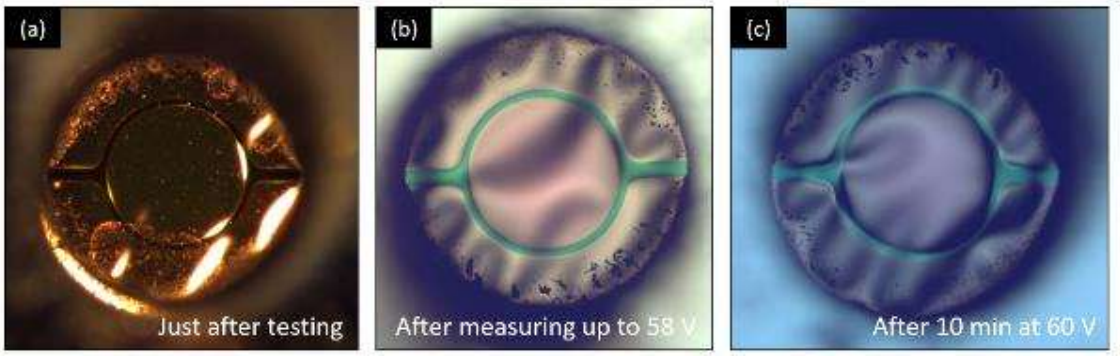

Figure 29: D4 heater (a) right after tests at Volvo, (b) after one round of measurements, (c) after 10 mins

Post resistance measurements, the two devices, D1 and D4, are subjected to constant power for specific duration. After each duration, the samples are optically characterized. The details of characterization are seen in Figure 28(a) for D1 and Figure 28(b) for D4. For D1, the total coverage of soot particles right after testing over the entire window area is 41 % (Figure 27(a)). After resistance measurements, the area of soot decreases to 27 % (Figure 27(b)). After 10 mins at 60 V, the soot area reduces to 18 % as shown in Figure 27(c). Since, the inner ring of the window

as completely clean, we moved to conduct the same measurements on D4. The area of soot is calculated as the ratio of measured number of soot pixels and window area in ImageJ software.

The second device, D4, used for burn off experiments was not directly in-line of the pipeline. Therefore, we see a relatively lesser amount of soot deposition compared to in-line windows shown in Figure 29(a). As we see in Figure 29(a), the optical inspection of total area covered by the soot on the windows is 60 % just after testing. The time between taking the image and testing the device is about 10 days. D4 is subjected to similar resistance measurements as D1 up to 58 V. The area of soot remaining after these measurements is 16 % (Figure 29(b)). When 60 V are applied on D4 for 15 min, the soot area reduces to 6 % (Figure 29(c)). The area of deposition reduces marginally when 60 V is applied for another 15 min as can be seen in Figure 29(d).

Discussion and conclusion

A key issue that has so far deterred automotive industry from using optical sensor systems in such a harsh an environment as the tailpipe is the contamination of sensing surfaces due to soot deposition. Addressing this issue is an important part of the project and we intend to systematically analyze the effectiveness of optical surface cleaning by periodical heating. The gained understanding in this aspect is expected to be of fundamental general strategic importance when it comes it considering industrial implementation of optical sensing systems.

In round 2, the updated design improved upon the stress distribution of the optically transparent membranes. The improved design demonstrated a robust mechanical characteristic during several runs of powering. The optical windows could reach up to 85 V over 1 min at 2 W without any damage to the windows. The design was later bounded on a high-temperature printed circuit board and encased in an aluminum housing designed to include an optical microscope in the future runs. The packages were tested for thermophoretic repulsion of soot to keep the windows clean and transparent during the measurement cycle and to clean the windows after every round of testing. Thermophoretic repulsion of soot particles was demonstrated by multiple soot accumulation experiments, where the die was parallel so the soot containing gas stream. There is a clear connection between the deposition of soot and biased device. The farther we go, the worse is the deposition. The windows can sustain a high voltage input (58 V) for about 66 minutes before breaking down. The engine test was a very sooty cycle (1 mg soot per kg air up to 700 – 800 peaks). Most of the soot can be burnt off the devices using 60 V for 20 – 25 mins with a clean hotspot area of 94 % after that duration. Device breakdown at high soot flow is still an issue that needs to be tackled. All the devices suffered damaged and rips after specific durations. The devices in round 1 burnt after only a few minutes at glowing temperatures. The devices in round 2, though more robust through simulations, still stops functioning after 2041 min at 43 V in an extremely sooty cycle, and 66 min for 60 V.

Publication list

The following publications are generated throughout the project:

Middelburg, Luke M., Mohammadamir Ghaderi, David Bilby, Jaco H. Visser, Guo Qi Zhang, Per Lundgren, Peter Enoksson, and Reinoud F. Wolffenbuttel. "Maintaining transparency of a heated MEMS membrane for enabling long-term optical measurements on soot-containing exhaust gas." Sensors 20, no. 1 (2020): 3.

References

[1] A.Malik, H. Abdulhamid, J. Pagels, J. Rissler, M. Lindskog, P. Nilsson, R. Bjorklund, P. Jozsa, J. Visser, A. Lloyd Spetz and M. Sanati, 'A potential soot mass determination method from resistivity measurement of thermophoretically deposited soot', Aerosol science and technology, (45), 2, 284-294, 2011.

[2] P. Intra and N. Tippayawong, 'An overview of aerosol particle sensors for size distribution and measurement', Maejo International J. Sci. & Tech. 01: 120-136, 2007.

[3] A. Rostedt, L. D. Ntziachristos, P. Simonen, T. Rönkkö, Z. C. Samaras, R. Hillamo, K. Janka, J. Keskinen, 'A New Miniaturized Sensor for Ultra-Fast On-Board Soot Concentration Measurements', SAE International Journal of Engines, 2017, 10, 1859-1865; doi:https://doi.org/10.4271/2017-01-1008.

[4] M. Feulner, G. Hagen, A. Müller, A. Schott, C. Zöllner, D. Brüggemann and R. Moos, 'Conductometric sensor for soot mass flow detection in exhausts of internal combustion engines', Sensors 2015, 15, 28796-28806; doi:10.3390/s151128796.

[5] G. Hagen, C. Feistkorn, S. Wiegärtner, A. Heinrich, D. Brüggemann and R. Moos, 'Conductometric Soot Sensor for Automotive Exhausts: Initial Studies', Sensors 2010, 10, 1589-1598; doi:10.3390/s100301589.

[6] D. Lutic and I. Cretescu, 'Detection of soot particles using a resistive transducer based on thermophoresis', Environmental Eng. And Management J., Vol. 13, No. 9, 2014.

[7] H. Zhaoa, B. Williams and R. Stone, 'Measurement of the spatially distributed temperature and toot loadings in a laminar diffusion flame using a cone-beam tomography technique', Journal of Quantitative Spectroscopy and Radiative Transfer, 133, pp. 136-152.

[8] M. K. Case and D. L. Hofeldt, 'Soot mass concentration measurements in diesel engine exhaust esing Laser-Induced Incandescence', Aerosol Science and Technology, 25:1, 46-60, 1996, DOI: 10.1080/02786829608965378.

[9] P. O. Witze, G. A. Payne, W. D. Bachalo and G. J. Smallwood, 'Influence of measurement location on transient Laser-Induced Incandescence measurements of Particulate Matter in raw diesel exhaust', 04ANNUAL-174, SAE, 2004.

[10] C.M. Keck and R.H. Muller, Size analysis of sub-micron particles by laser diffractometry – 90% of the published measurements are false, Int. J. of Pharmaceutics, 355 (2008) 150-163

[11] H. Jung and D. Kittelson, 'Measurement of electrical charge on diesel particles', Aerosol Science and Technology, 39:1129-1135, 2005, DOI 10.1080/02786820500430357.

[12] M. Fiebig, A. Wiartalla, B. Holderbaum and S. Kiesow, 'Particulate emissions from diesel engines: correlation between engine technology and emissions', J. of occupational medicine and toxicology, Vol. 9 No. 6, 2014.

[13] A.Emadi, H. Wu, G. de Graaf, and R. Wolffenbuttel, 'Design and implementation of a sub-nm resolution microspectrometer based on a Linear-Variable Optical Filter', Opt. Express, vol. 20, pp. 489-507, 2012.

[14] A.Emadi, H. Wu, S. Grabarnik, G. De Graaf and R. Wolffenbuttel, 'Vertically tapered layers for optical applications fabricated using resist reflow', Journal of Micromechanics and Microeng., vol. 19, p. 074014, 2009.G.